Polymer xxx (xxxx) 125826

Contents lists available at ScienceDirect

Polymer

journal homepage: www.elsevier.com/locate/polymer

Reaction-Induced structural and compositional heterogeneity in amine-cured epoxy/epoxy thermosets: Visualization of heterogeneity using fluorescence lifetime imaging microscopy (FLIM)

Jeremiah W. Woodcock **, Stephan J. Stranick, Anthony P. Kotula, Shawn H. Chen, Jeffrey W. Gilman, Gale A. Holmes *

National Institute of Standards and Technology, Materials Science and Engineering Division, 100 Bureau Drive Stop 6421, Gaithersburg, MD, 20899, USA

A B S T R A C T

The strategic integration of a rhodamine-spirolactam (RS) mechanophore into transparent epoxy-amine (E-A) networks has revealed using fluorescence lifetime imaging microscopy (FLIM), multiple domains in the cured epoxies that are different (compositional and structural heterogeneity) even though only a single glass transition temperature (T_g) is observed in the solid rheology data. For the E-A networks investigated in this study, the FLIM data suggests that heterogeneity exists at two levels (molecular and macroscopic). Heterogeneity in the network composed of diglycidyl ether of bisphenol-A (DGEBA) epoxy cured with meta-phenylenediamine (m-PDA) is associated with the network being under-cured. In the network composed of the diglycidyl ether of 1,4-butanediol (DGEBD) cured with m-PDA, heterogeneity is linked to the oligomers that likely self-associate in the 60 mass % DGEBD medium, thereby creating discrete regions of low crosslink density in the cured network. In the DGEBA (80 mass %)/DGEBD (20 mass %) epoxy blend cured with m-PDA, the heterogeneous morphology in this fully cured network is caused by reaction kinetics differences of the two miscible bis-epoxides with m-PDA at the molecular level and the self-association of the oligomers found in the 60 mass % DGEBD medium at the macroscopic level.

1. Introduction

The question of heterogeneity in thermoset systems has been an area of research interest for at least the last 45 years, with the primary investigative tools being small-angle X-ray scattering, small-angle neutron scattering, light scattering, magnetic birefringence, stress birefringence, nuclear magnetic resonance, electron paramagnetic resonance, scanning electron microscopy (SEM), scanning transmission electron microscopy (STEM), and fluorescence spectroscopy [1–3]. Researchers have also relied on information based on the network formation process, with particular emphasis placed on (a) reaction kinetics, (b) distribution of oligomeric species, (c) network build-up parameters, and (d) controlled molecular architecture studies [3–6]. In 1996, Dusek deduced that thermoset resin heterogeneity for systems cured by simple stepwise alternating chemistries fulfills the network homogeneity criterion, provided there is good compatibility of components [3]. He concluded that epoxy resins cured with polyamines [i.e., epoxy-amine (E-A) networks] belongs to this category.

Due to the importance of thermoset systems in structural applications, this continues to be an active area of research with efforts focused on linking the structure of the network to its mechanical properties, thereby ensuring the effective use of these materials in the targeted application [6,7]. Since many of these thermoset networks are transparent, new measurement tools are continually being developed to illuminate the network structure, with recent research efforts focused on using atomic force microscopy-infrared spectroscopy (AFM-IR) to detect nano-structural heterogeneities [8], tapping mode AFM to detect heterogeneities [9], and the use of fluorescent dye labeled polystyrene particles to track heterogeneity during the cure process [10]. It must be noted that all these evaluations are done on length scales of <1 μm, which we term molecular level heterogeneity in the publication.

Prior research on the aromatic epoxy/aliphatic epoxy blend cured with a cycloaliphatic diamine [11,12] is used to anticipate the expected macroscopic heterogeneities. The unequal reactivities of the aromatic and aliphatic epoxide with the amine led the cited researchers to postulate DGEBA-amine rich and DGEBD-amine rich regions in the network. Since the cure behavior of the unblended E-A systems should conform to the auto-catalyzed mechanism put forth by the highly-cited research of I.T. Smith (Scheme 1) [13] and the well-cited reaction kinetics study by Dusek (Scheme 2) [14], these schemes provide the basis for understanding the development of molecular level heterogeneities.

* Corresponding author.
** Corresponding author.
E-mail addresses: Jeremiah.woodcock@nist.gov (J.W. Woodcock), gale.holmes@nist.gov (G.A. Holmes).

https://doi.org/10.1016/j.polymer.2023.125826
Received 21 October 2022; Received in revised form 16 February 2023; Accepted 25 February 2023
0032-3861/© 20XX

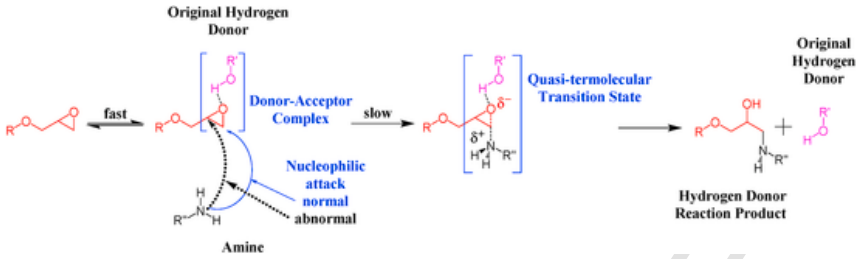

Scheme 1. Epoxy-Amine autocatalytic reaction scheme proposed by I.T. Smith [13].

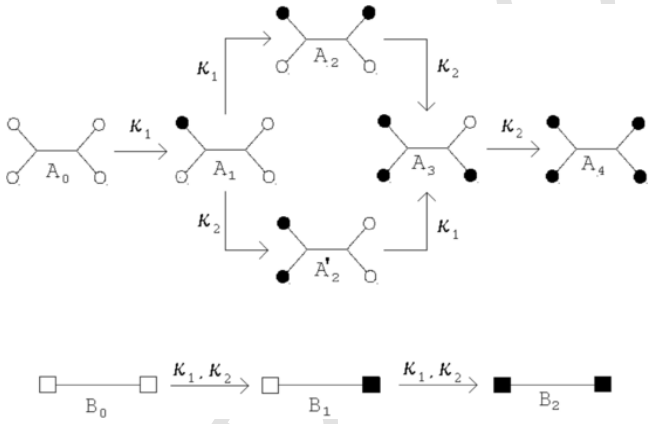

Scheme 2. Kinetics of curing diepoxide (B_is) with diamine (A_is) for fractions of monomer units with different number of reacted functionalities. *(Adapted from* Ref. [14]*).*

A critical feature of Scheme 1 is the requirement that a hydrogen bond donor molecule (e.g., alcohols, phenols, acids) must be present for the E-A reaction to proceed. Secondly, the initial hydrogen bond donor molecule is recovered, thereby allowing it to catalyze the reaction of additional epoxide groups. Furthermore, the E-A reaction product also contains a hydroxyl group that further increases the concentration of hydrogen bond donor molecules. Hence, the E-A reaction is known to be autocatalytic. From the early research of Shechter et al. [15] and Rozenberg [16] it is known that the E-A reaction in Scheme 1 is dominant and that the possible competing reaction of epoxide with hydroxyl groups is not detected in E-A network reactions that are slightly amine rich.

The E-A reaction kinetics depicted in Scheme 2 plays a critical role in understanding the observed molecular level heterogeneities that may be observed. In this scheme, the molecular network build-up is dependent on the reaction rates of the primary and secondary amines (i.e., A_is) with the bis-epoxides (B_is). For aromatic amines (e.g., m-PDA) reacting with epoxides, the primary amine reaction rate (K_1) is greater than the secondary amine reaction rate (K_2). Thus, the epoxy-aromatic amine network build-up undergoes preferential extension of the polymer chain (upper pathway) prior to the formation of crosslinks (A_3). In contrast, network build-up in epoxy-aliphatic amine networks is different since $K_1 \approx K_2$, which indicates that both pathways are equally likely [14,16]. It must be noted that the reaction of the epoxides on B_is are considered to be independent, due to the typically large spacing between the two epoxides.

Scheme 2 also implies that the epoxy/epoxy/amine networks where the two epoxides react concurrently with the amine but at different rates are inherently heterogeneous at the molecular level, except for possibly at the beginning and end of the E-A reaction. Thus, most of the reacted A_i species are unlikely to be reacted with the same bis-epoxide.

In this publication, a novel molecular fluorescence probe, which is sensitive to the microenvironment surrounding the molecule [17], is strategically integrated into E-A thermoset networks and fluorescent lifetime imaging microscopy (FLIM) is used to detect heterogeneities at the molecular and macroscopic level. An epoxy/reactive diluent blend was chosen for study that is widely used in composite manufacturing [18]. Specifically, diglycidyl ether of bisphenol-A (DGEBA, Epon 828, Figure SI 1) and diglycidyl ether of 1,4-butanediol (DGEBD, Araldite RD-2, Figure SI 2) were blended in an 80/20 mass % ratio and cured with meta-phenylenediamine (m-PDA). For comparison, the unblended networks were also cured with m-PDA.

2. Experimental

2.1. Component materials

The diglycidyl ether of bisphenol-A [DGEBA, Epon828,[1] purity = (77.1–82.3) mass % [19,20], epoxide equivalent weight (EEW) = 185–192 g/eq and analytical grade DGEBA, purity ≈ 100 mass %, EEW = 170–175 g/eq], the diglycidyl ether of 1,4-butanediol (DGEBD, Araldite RD-2, purity ≈ 60 mass %, EEW = 120–140 g/eq [20] and 95 mass % DGEBD) and meta-phenylene diamine (m-PDA, purity = 99+ mass %, amine hydrogen equivalent weight (AHEW) = 27.03 g/eq) were purchased from Sigma-Aldrich and used as received. The procedure for synthesizing the quenched RS-mechanophore shown in Scheme 3 has been published [21].

[1] Certain commercial equipment, instruments, or materials are identified in this document. Such identification does not imply recommendation or endorsement by the National Institute of Standards and Technology, nor does it imply that the products identified are necessarily the best available for the purpose.

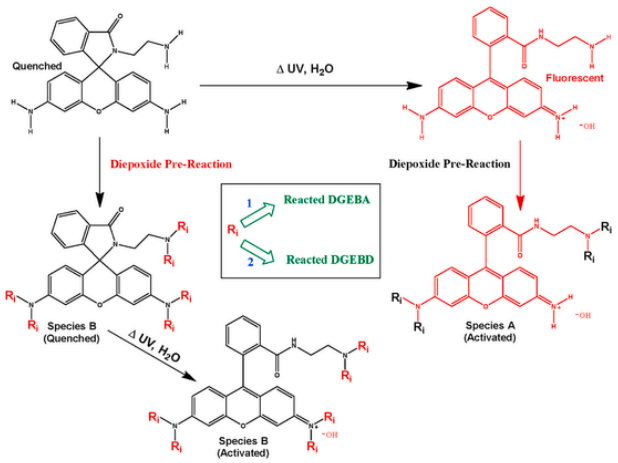

Scheme 3. Pre-reaction of rhodamine-spirolactam (RS) mechanophore (quenched and UV activated) with targeted bis-epoxides (DGEBA and DGEBD).

2.2. Controlling the Mechanophore's reaction kinetics and insertion into epoxy-amine (E-A) networks

To control the reaction kinetics, the mechanophore was pre-reacted with excess bis-epoxide at 80 °C to eliminate the amine reaction kinetics from consideration, since the mechanophore's aliphatic and aromatic amines (Scheme 3) react with epoxides at different rates [22]. By end-capping the mechanophore amine groups with the targeted bis-epoxide, insertion of the mechanophore into the network is controlled by the unreacted epoxides of the targeted bis-epoxide. Based on the known E-A reaction kinetics deduced by I.T. Smith (Scheme 1) [13], the pre-reacted RS-mechanophore will react similarly to the targeted bis-epoxide in the E-A reaction, albeit a slight acceleration in reaction kinetics due to the additional hydroxyl groups [22]. The appropriate amounts of bis-epoxide were then added to achieve a 0.47 mass % targeted amount of mechanophore in the dogbone specimens. DGEBA was chosen as the targeted bis-epoxide for the DGEBA/DGEBD blend since it reacts faster than DGEBD. Because DGEBA (Figure SI 1) and DGEBD (Figure SI 2) contain oligomers with hydroxyl groups, the pre-reacted mechanophore is not expected to significantly accelerate the reaction kinetics at the targeted 0.47 mass % level. The prepared resin systems are in Table 1.

2.3. Specimen preparation procedure

Test specimens were prepared by filling silicone rubber molds following a previously described procedure that is briefly discussed below [24]. All molds were rinsed with acetone and heated to remove acetone prior to use.

One hundred grams of mechanophore labeled DGEBA, DGEBD, or the DGEBA (80 mass %)/DGEBD (20 mass %) epoxy blend were weighed out in a beaker. A stoichiometric amount plus 6% excess of m-PDA was weighed in a separate beaker. Although the excess curative slightly decreases the crosslink density in the final cured network, industrial knowledge suggests that in fully-cured E-A networks it virtually eliminates the presence of un-reacted epoxides in the network, thereby minimizing the potential side reaction of un-reacted epoxides with alcohols during the diffusion control region of the cure, and results in slightly better network properties (e.g., increased rupture strain [25]). The beakers were placed in separate vacuum ovens at 65 °C to degas the resin and to melt and degas the curative. The silicone rubber molds were preheated to the initial curing temperature to dry the molds and minimize the formation of air bubbles during the curing process. Approximately 9 min before the preheated molds were removed from the oven, the DGEBA, DGEBD, or DGEBA/DGEBD blend was removed from the oven. The melted and degassed m-PDA was then removed from the oven and poured into the epoxy and mixed thoroughly. The mixture was placed into the vacuum oven used to melt the curative and degassed for approximately 7 min. The preheated molds were removed from the oven and filled with the resin/curative mixture using 10 ml disposable syringes. The filled molds were then placed into a programmable oven (Blue M, General Signal, Model MP-256-1, GOP).

In a previous publication [23] the DGEBA (80 mass %)/DGEBD (20 mass %)/m-PDA network was cured using the following cure schedule (CS): 60 °C (3 h) + 121 °C (2 h). In that research it was discovered that the network was slightly under-cured. To remove the contribution of dangling ends from the observed fluorescence lifetimes in the DGEBA (80 mass %)/DGEBD (20 mass %)/m-PDA network, the CS was modified to 60 °C (3 h) + 121 °C (2 h) + 130 °C (1 h). This cure schedule change is not expected to alter the network morphology or its properties. The interested reader can compare the morphologies of the DGEBA (80 mass %)/DGEBD (20 mass %)/m-PDA networks shown in Figure SI 3 (Supplemental Information: Hyperspectral Response of Mechanophore Section), which was obtained with the previous CS, and Fig. 8 that is obtained using the current CS. To eliminate the CS as a variable the modified CS is used for all specimens in this study.

Table 1
Mechanophore labeled Epoxy/m-PDA Systems.

System	Mass % Epoxy Components		T_g, °C [23]
	DGEBA	DGEBD	
1M	100		138
2M(a)		100 (60% purity)	≈60
2M(b)		100 (95% purity)	≈60
3M	80	20	130

2.4. Fluorescence lifetime image microscopy (FLIM) measurements

The in-house built time-correlated single photon counting (TCSPC) instrument with 140 fs pulse laser system was used to characterize the RS-mechanophore labeled E-A specimens. The apparatus used for fluorescence lifetime determination is described in detail elsewhere [21]. Samples were imaged approximately 50 μm below the specimen surface using two photon excitation at 810 nm with a 40 ms dwell time under stage restoring, and an air objective with a numerical aperture of 0.9. The thickness of each image is ≈ 1 μm. Following the fluorescence decay fits, after appropriate binning of the photon counts at each pixel for a 256x256 pixel image (at a 300 × 300 μm image size), fit parameters and the corresponding images were exported from the SPCImage software.

During the internal review of this manuscript, it was acknowledged that in a previous publication [21] the hyperspectral trace of the RS-mechanophore exhibited two fluorescent centers that we labeled Species A and B (Scheme 3, for details see Supplemental Information: Hyperspectral Response of Mechanophore Section). The reviewer suggested that these two fluorescence centers may necessitate the need to fit the decay curve shown in Fig. 1 with a double exponential function (DEF).

Even though we are not concerned with the fiber interphase in this paper, some extra calculations and analysis were performed to show that phase separation of species A and B are not an issue. Secondly, we solidify this assertion with experimental data presented in the DGEBD/m-PDA [System 2 M(a) and (b)] section. Specifically, we show that the decay curve for the high-purity DGEBD/m-PDA [2 M(b)] network is readily fit using a single exponential function (SEF), while the low-purity 2 M(a) network requires the DEF.

The standard convolution integral (Equation 1) is applied to each decay curve pixel by pixel to obtain $f_m(t)$ for each pixel. However, there is no analytical expression to obtain $f(\tau)$ in Equation 1. Multiple groups

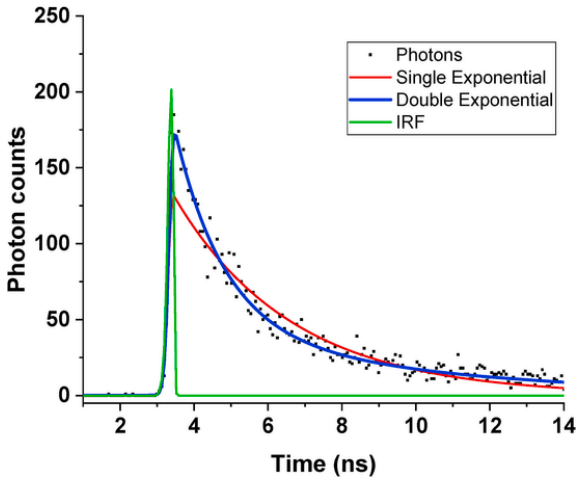

Fig. 1. Representative lifetime decay curve fit using both the single and double exponential fit model for f(τ). This is used in each pixel by the Becker and Hickl algorithm. The measured instrument response function (IRF) is shown in green and the fits in red and blue. (For interpretation of the references to color in this figure legend, the reader is referred to the Web version of this article.)

have used a stretched exponential function (STrEF) to fit lifetime decay curves in complex biological systems where a broad distribution of microenvironments exists [26–29]. As a result, the distribution of decay lifetimes is also broad, and the STrEF provides a simple description of the complex relaxation processes in those materials. In contrast, prior studies on epoxy/epoxy/amine thermosets have hypothesized that the network morphology has a two-domain microstructure [11,12,30]. Thus, we propose that fitting the fluorescence decay curve with a DEF may provide a more insightful characterization of the relaxation processes in the cured samples studied in this work.

Equation 1. Convolution integral with instrument response function

$$f_m(t) = \int_{t=0}^{t} f(\tau)\, IRF(t-\tau)\, d\tau$$

where

$f_m(t)$ – measured fluorescence function
$f(\tau)$ – true exponential decay function

$$\text{Single exponential} = f(\tau) = e^{\frac{-t}{\tau}}$$

$$\text{Double exponential} = f(\tau) = a_1 e^{\frac{-t}{\tau_1}} + a_2 e^{\frac{-t}{\tau_2}}$$

IRF(t) – Instrument response function

In all the data presented here, the detected lifetime decay for each pixel volume, which contains the emission from $\approx 440,000$ mechanophore molecules, was fit using a SEF or a DEF. In one case (specifically, the DGEBD (95 mass %)/m-PDA network), a SEF provided a good fit to the data so the lifetime within each pixel could be characterized by τ^{SP}, where "*SP*" denotes single pixel. This means that the local environment surrounding all the mechanophore units (i.e., within each pixel) is the same. Since all have the same lifetime response, this suggests the material is homogeneous in that region at the molecular level and given that all the pixels in the image have a similar distribution, macroscopic homogeneity is indicated.

On the other hand, as illustrated in Fig. 1, the lifetime decay curves for the remaining systems could not be parameterized within each pixel using a SEF. Given that an exponential decay is proportional to the population of photons from a given emitter, the presence of multiple population of emitters will necessitate additional exponential expressions to fit the curve through the linear combination of the exponentials. This indicates in each pixel different local environments surrounding the mechanophore or heterogeneity at the molecular level. A DEF provided a good fit of the data for the remaining networks. As has been noted in previous studies [31,32], however, the possibility of more than two exponentials cannot be eliminated based on these fits alone because additional terms provide essentially the same fit curve. Nevertheless, within each pixel the DEF fit allows the response to be characterized by two lifetimes denoted τ_1^{SP} and τ_2^{SP}. The difference between the two provides an indication of heterogeneity at the molecular (sub-pixel) level. The weighted average, τ_m^{SP}, indicates the average lifetime within each pixel. When the average lifetimes in adjacent pixels are about the same, this indicates macroscopic regions of similar cure behavior. Thus, color changes in τ_m^{SP} between multiple pixel regions indicate macroscopic heterogeneity. The question that arises from these image changes is: "What factors influence macroscopic heterogeneity?"

The software algorithm using the selected model performs a best fit in each pixel to obtain the lifetime for the emitters. The pixels are fit and deconvoluted independently. Examples of the fits for the investigated systems are shown in the Supplemental Information: Single Pixel Analyses Section and discussed in the Discussion Section under their appropriate headings. A histogram showing the distribution of these fits can be plotted and a false color-coded image is obtained. Through this methodology, heterogeneity in local dynamics can be visualized. The image plots are presented using τ_m^{SP} values from each pixel, which is the intensity-weighted mean of lifetimes τ_1^{SP} and τ_2^{SP} within each pixel [31,33,34]. This will result in the value observed in a pixel to be proportional to the quantum efficiencies of the emitters it contains. A true average disregards this information and can be biased to the most populous emitter. Examples of histograms generated by the τ_m^{SP} from each pixel are presented in the Discussion Section for the systems investigated.

3. Theoretical calculations

Solubility Parameter Calculations. The First level thermodynamic estimates [35] of each system are obtained by calculating the solubility (δ_i) parameters of the monomers and δ_i of key structural elements formed during the curing process. This is done primarily using the Yamamoto-Molecular Breaking (Y-MB) method embodied in the Hansen Solubility Parameters in Practice (HSPiP) software (version 5.3.07) or manually as shown in the Supplemental Information: First Level Thermodynamic Estimates of Reactant Species Section. Given the difficulty in predicting miscibility [36], evaluations are done manually. Estimates of refractive index (RI) are also obtained from the Y-MB method and where possible compared with experimental data.

Density Functional Theory (DFT) Calculations. DFT calculations were performed to assess the change in polarizability caused by changes in molecular structure of the RS mechanophore (see Supplemental Information: Hyperspectral Spectral Response of Mechanophore Section). These calculations were performed with Spartan 16 software using the B3LYP hybrid functional model [37] and the 6-31G* basis set [38].

4. Results and discussions

DGEBA/m-PDA [System 1 M] Network. For the mechanophore labeled DGEBA/m-PDA network shown in Fig. 2A the false color 50 × 50 μm image is displayed with a τ_m lifetime window from 2.5 ns to 4.5 ns. Based on the DEF used to analyze each pixel, the τ_m^{SP} values are deconvoluted into τ_1^{SP} and τ_2^{SP} values and histogram plots of each are shown in Fig. 2B. The τ_1^{SP} values cover a range from $\tau_1^{SP} \approx 0.7$ ns to $\tau_1^{SP} \approx 2.1$ ns to yield a mean (i.e., $\langle \tau_1 \rangle$) of 1.43 ns, while the mean of the

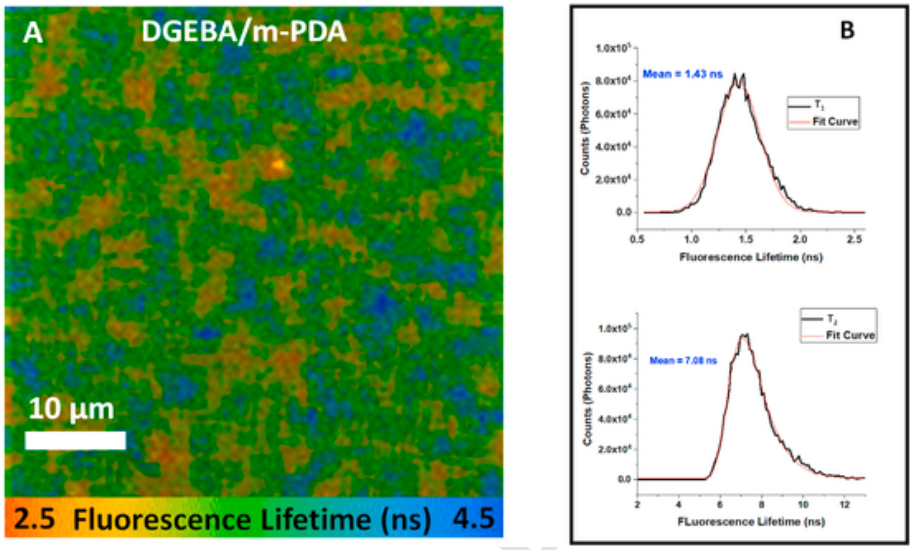

Fig. 2. (A) False color image for the photoactivated mechanophore contained in epoxy resin DGEBA/m-PDA to allow visualizing the dynamic heterogeneity of the matrix. The photon counts from each pixel (τ_m^{SP}) is based on the weighted average fluorescence lifetimes components (τ_1^{SP} and τ_2^{SP}) from the DEF. (B) Histograms for the fluorescence lifetime components [τ_1^{SP}, with mean value $\langle\tau_1\rangle = 1.43$ ns, and τ_2^{SP}, with mean value $\langle\tau_2\rangle = 7.08$ ns). Lower lifetimes are indicative of regions with faster local dynamics. (For interpretation of the references to color in this figure legend, the reader is referred to the Web version of this article.)

τ_2^{SP} values (i.e., $\langle\tau_2\rangle$) is 7.08 ns with values ranging from $\tau_2^{SP} \approx 5.4$ ns to $\tau_2^{SP} \approx 11.0$ ns. These sub-pixel (<1.17 µm) responses from the RS-mechanophores indicate a mixture of local environments that contain fast (represented by τ_1^{SP}) and slow (represented by τ_2^{SP}) molecular dynamics at the molecular level. Most recently, sub-pixel heterogeneity (<1 µm) has also been observed during the room temperature curing dynamics for hydrogenated DGEBA (HDGEBA) reacted with 1,4-cyclohexane bis(methylamine) [10]. These researchers used fluorescent labeled polystyrene particles to sense changes in localized mobility on the length scale of several hundred to tens of nanometers during the curing process, which they labeled mesoscopic heterogeneity. They concluded that the origin of this heterogeneity results from the localized temperature rise due to the heat of formation when an epoxy and amine group react. This temperature rise accelerates a subsequent reaction nearby. Repeating such a situation results in unevenly reacted domains being formed.

The molecular level heterogeneity observed in this study is also consistent with the findings of Gupta et al. [1] who used the following CS for the DGEBA/m-PDA network: 75 °C (2 h) + 125 °C (2 h). Their SEM results (Fig. 7 in Ref. [1]) revealed heterogeneities in the range 5–100 nm in the 1.18 × 1.76 µm image. Additionally, STEM of an osmium tetraoxide stained sample revealed the existence of low crosslinked density regions (Figure 11 in Ref. [1]). Noting that Gupta's images are about the size of 1 pixel in this study or less, the heterogeneity observed in their network is consistent with the DEF fit of the fluorescence signal emanating from each pixel in this study, which we are calling molecular level heterogeneity. Consistent with the research of Gupta et al. [1,39], additional research [23] indicates that the CS used in this report leads to the DGEBA/m-PDA network also being under-cured. The known E-A cure kinetics (Scheme 2) [13,14] implies that under-curing results in a network that contains a mixture of A_{2-4} linkages at the molecular level.

To illustrate how the DGEBA/m-PDA network evolves when it is fully-cured, a post-cure procedure similar to that used by Gupta et al. [39] was followed. Specifically, the DGEBA/m-PDA network in this report was post-cured a 175 °C for 2.5 h under vacuum, which brought the system closer to complete cure. Relative to the under-cured network in Fig. 2, $\langle\tau_1\rangle$ increased slightly, while $\langle\tau_2\rangle$ decreased dramatically (Fig. 3). Although the regions are smaller, the system remained heterogeneous at the molecular and macroscopic levels.

Additionally, in Fig. 4, histogram plots of the τ_m^{SP} values are shown for the under-cured DGEBA/m-PDA network along with similar distributions from the soon to be discussed DGEBD (60 mass % purity)/m-PDA and DGEBA (Epon 828, 80 mass %)/DGEBD (Araldite RD-2, 20 mass %)/m-PDA networks. For the DGEBA/m-PDA network the mean value of τ_m^{SP}, (i.e., $\langle\tau_m^{SP}\rangle$) is ≈ 3.6 ns with a τ_m^{SP} range from ≈ 3.2 ns to ≈ 4.0 ns. A comparison of the τ_m^{SP} histogram to the τ_1^{SP} and τ_2^{SP} histograms in Fig. 2B indicate that $\langle\tau_1\rangle$ and $\langle\tau_2\rangle$ and their respective ranges are outside the range of the DGEBA/m-PDA network τ_m^{SP} data. Based on the DEF model, each τ_m^{SP} value is therefore a sum of τ_1^{SP} and τ_2^{SP} values, thereby reflecting the molecular level heterogeneity in each pixel that was discussed above.

Interestingly, the false color image in Fig. 2 suggests heterogeneity on a scale of about 10 μm that is much larger than previously reported. Each distinct region has multiple pixels that have similar molecular level compositions. To illustrate this point, in Fig. 2A at least three distinct regions are apparent: (1) dark blue (long lifetime) regions that are ≈ 2 µm in size and having τ_m lifetimes of ≈ 4.5 ns or higher, (2) light blue to green (intermediate lifetime) regions ≈ 10 µm in size with τ_m lifetimes of about 3.0 ns to 3.5 ns, and (3) brownish (short lifetime) regions ≈ 5 µm to ≈ 7 µm in size with a τ_m lifetime of ≈ 2.5 ns. A single pixel from each region was analyzed with the selected pixel shown in the Supplemental Information (SI, Figure SI 8) and the results summarized in Table 2.

From Table 2, it is readily apparent that τ_1^{SP} and τ_2^{SP} values and their photon fraction vary from pixel to pixel. From the DGEBA/m-PDA τ_m^{SP} histogram plot shown in Fig. 4, the pixels in each distinct region do not reflect a unique combination of τ_1^{SP} and τ_2^{SP} values and corresponding photon fractions but rather represents the many combinations of τ_1^{SP} and τ_2^{SP} values and their corresponding photon fractions that combine to yield pixels with similar τ_m^{SP} values. These similar values of τ_m^{SP} in Fig. 2, which are heterogeneous on the molecular level, forms the basis for the macroscopic heterogeneity that is observed. Furthermore, the data in Table 2, suggests that slowing of the molecular dynamics at the pixel

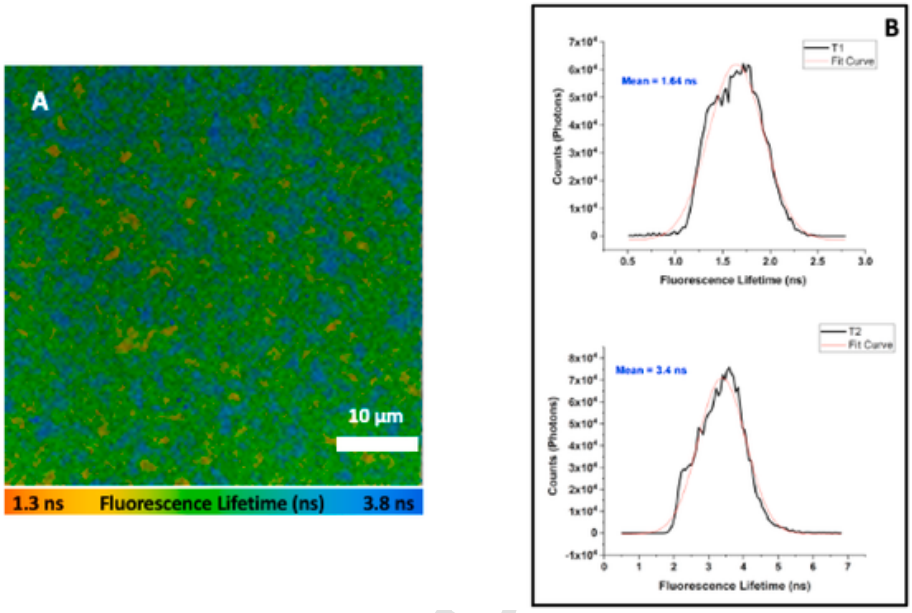

Fig. 3. (A) False color image for the photoactivated mechanophore contained in epoxy resin DGEBA/m-PDA post cured at 175 °C for 2.5 h under vacuum to allow visualizing the dynamic heterogeneity of the matrix. The photon counts from each pixel (τ_m^{SP}) is based on the weighted average fluorescence lifetimes components (τ_1^{SP} and τ_2^{SP}) from the DEF. (B) Histograms for the fluorescence lifetime components [τ_1^{SP}, with mean value $\langle\tau_1\rangle = 1.64$ ns, and τ_2^{SP}, with mean value $\langle\tau_2\rangle = 3.4$ ns). Lower lifetimes are indicative of regions with faster local dynamics. (For interpretation of the references to color in this figure legend, the reader is referred to the Web version of this article.)

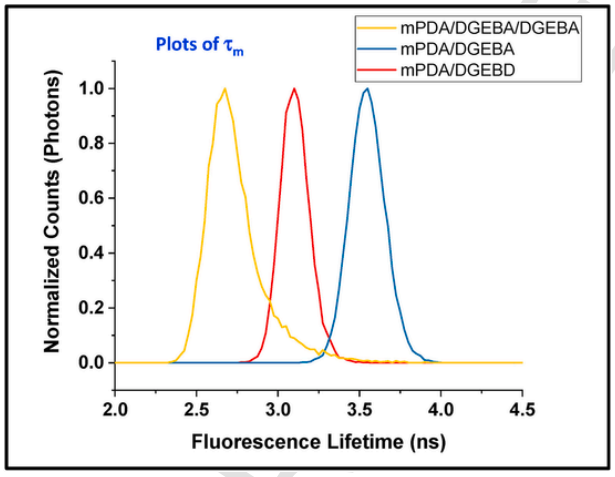

Fig. 4. Histograms for the averaged lifetime distributions for three epoxy formulations containing photoactivated mechanophore [DGEBA/m-PDA (blue), 60 mass % DGEBD/m-PDA (red) and DGEBA (80 mass %)/DGEBD (20 mass %)/m-PDA (yellow)]. (For interpretation of the references to color in this figure legend, the reader is referred to the Web version of this article.)

Table 2
Selected single pixel analyses from DGEBA/m-PDA network.

False Color Region in Fig. 2 System 1 M	Figure SI 8 Analysis Code	τ_m^{SP}	τ_1^{SP}		τ_2^{SP}	
			ns	Photon Fraction	ns	Photon Fraction
Dark Blue	D	3.8	1.7	0.661	7.9	0.339
Light Blue to Green	B	3.7	1.5	0.569	6.6	0.431
Brownish	C	3.3	1.1	0.511	5.6	0.489

level, which is reflected by increasing τ_m^{SP} values, is not simply correlated at the molecular level to increasing values of τ_2^{SP} (i.e., the slow molecular dynamics parameter) and a corresponding increase in its photon fraction. Interestingly, while both τ_1^{SP} and τ_2^{SP} increase as τ_m^{SP} increases the photon fraction of τ_1^{SP}, which represents faster molecular dynamics, increases rather than the photon fraction of τ_2^{SP}, which represents slower molecular dynamics. Since τ_1^{SP}, reflects regions of increasing dynamic mobility, the increase appears counterintuitive with decreasing mobility on the pixel level. Finally, based on these data, the use of τ_1^{SP} and τ_2^{SP} values from the DEF to capture the molecular dynamics of the low- and high-crosslinked density regions seems reasonable for this system. However, the concurrent increase of τ_m^{SP} and τ_1^{SP} and its corresponding photon fraction, warrants further research.

DGEBD/m-PDA [Systems 2 M(a) and (b)]. In Fig. 5A, the τ_m lifetime window for the false color image of the mechanophore labeled DGEBD (60 mass % purity)/m-PDA [2 M(a)] network ranges from 1.9 ns to 2.8 *ns* and readily reveals evidence of macroscopic heterogeneity.

Given the evidence of macroscopic heterogeneity, the FLIM signal from each pixel (τ_m^{SP}) was found to be best fit by the DEF. Histogram plots of the deconvoluted τ_1^{SP} and τ_2^{SP} values are shown in Fig. 5B. From the plots, $\langle\tau_1\rangle = 1.39$ ns (range: $\tau_1^{SP} \approx 0.9$ ns to $\tau_1^{SP} \approx 1.9$ ns) and $\langle\tau_2\rangle = 5.9$ ns (range: $\tau_2^{SP} \approx 4.9$ ns to $\tau_2^{SP} \approx 9.0$ ns). Like the DGEBA/m-PDA network, the range for the $\langle\tau_1\rangle$ and $\langle\tau_2\rangle$ values are outside the range of τ_m^{SP} values (≈ 2.5 ns to ≈ 3.5 ns in Fig. 4). Therefore, each τ_m^{SP} value is composed of τ_1^{SP} and τ_2^{SP} values and the sub-pixel responses from the RS-mechanophores indicates a mixture of local environments that contain fast (represented by τ_1^{SP}) and slow (represented by τ_2^{SP}) molecular dynamics. Similar to the analysis in the previous section, a pixel was selected from each of the two distinct (green and brownish/orange) regions in Fig. 5A and analyzed (Figure SI 9) with the tabulated results in Table 3 consistent with molecular level heterogeneity on the sub-pixel level.

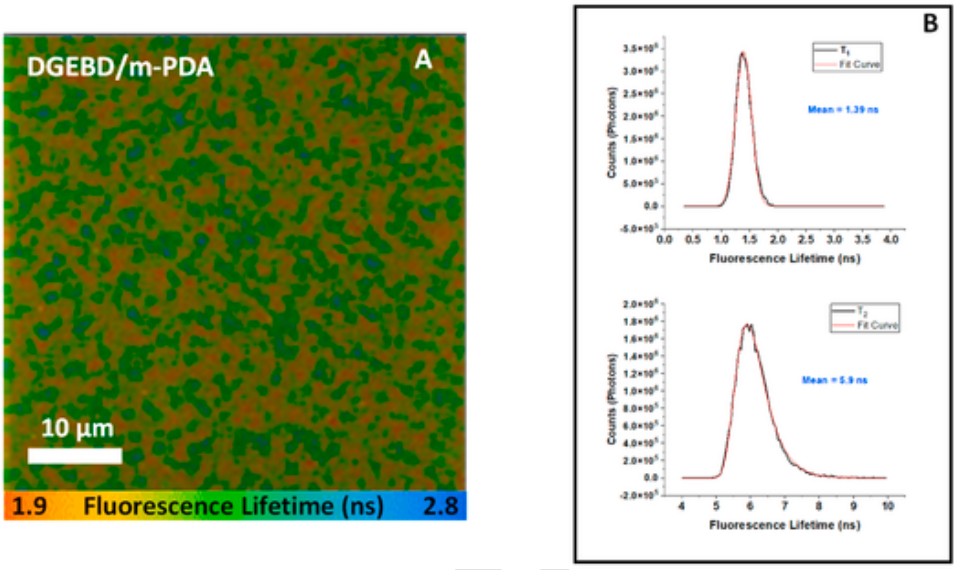

Fig. 5. (A) False color image for the photoactivated mechanophore contained in epoxy resin DGEBD (60 mass % purity)/m-PDA to allow visualizing the dynamic heterogeneity of the matrix. The photon counts from each pixel (τ_m^{SP}) is based on the weighted average fluorescence lifetimes components (τ_1^{SP} and τ_2^{SP}) from the DEF. (B) Histograms for the fluorescence lifetime components [τ_1^{SP}, with mean value $\langle \tau_1 \rangle = 1.39$ ns, and τ_2^{SP}, with mean value $\langle \tau_2 \rangle = 5.90$ ns). Lower lifetimes are indicative of regions with faster local dynamics. (For interpretation of the references to color in this figure legend, the reader is referred to the Web version of this article.)

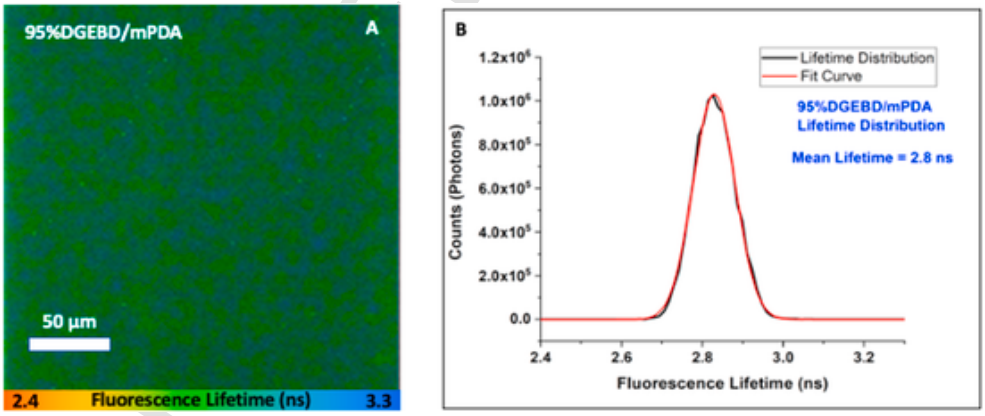

Fig. 6. (A) False color image for the photoactivated mechanophore contained in epoxy resin DGEBD (95 mass % purity)/m-PDA to allow visualizing the dynamic heterogeneity of the matrix. The photon counts from each pixel (τ_m^{SP}) is based on the fluorescence lifetime component (τ^{SP}) from the SEF. (B) Histogram for the fluorescence lifetime components [τ^{SP}, with mean value $\langle \tau^{SP} \rangle = 2.8$ ns). The single lifetime is indicative of homogeneous local dynamics. (For interpretation of the references to color in this figure legend, the reader is referred to the Web version of this article.)

As before, the repeat values of τ_m^{SP} for the DGEBD/m-PDA histogram plot (Fig. 4) do not reflect a unique combination of τ_1^{SP} and τ_2^{SP} values and corresponding photon fractions but rather represents the many combinations of τ_1^{SP} and τ_2^{SP} values and their associated photon fractions that combine to yield pixels with similar τ_m^{SP} values. Due to the presence of oligomers in the DGEBD (60 mass % purity, Figure SI 2), it follows from Scheme 2 that molecular level heterogeneity in this system is likely, since the co-reaction of DGEBD oligomers and the predominant DGEBD ($m = 0$) monomer should alter the crosslink density of the network in a random manner at the molecular level. However, what is not clear from Scheme 2 is the presence of the macroscopic heterogeneity observed in Fig. 5A.

Origin of the Macroscopic Heterogeneity Observed in the DGEBD (60 mass % purity)/m-PDA [2 M(A)] Network. The macroscopic heterogeneity in the DGEBD (60 mass % purity)/m-PDA [2 M(A)] network is presented in Fig. 5A as green (≈ 3.0 ns) regions and brownish/orange (≈ 2.0 ns) regions that resemble interconnected aspherical domains. Recalling that the distribution of oligomeric species may affect network heterogeneity, it was hypothesized that the two-phase morphology may be due to the presence of the 40 mass % of oligomers in the crude DGEBD. The analysis of RD-2 (60 mass % DGEBD) by Pearce and Mijovic [20] indicates that this material is composed of $n = 0, m \leq 3$ oligomers (Supplemental Information Figure SI 2). The synthesis chemistry of aliphatic bis-epoxides [40], also indicates that hydrolysable chloride content in crude DGEBD ($n = 1$ in Supplemental Information Figure SI 2) can be $\approx 0.1\%$. A First level thermodynamic

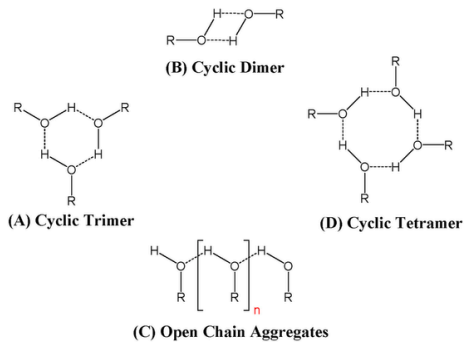

Fig. 7. A schematic presentation of the various self-associating alcohol structures *(Adapted from* Refs. [42,43]*)*.

miscibility check of these oligomers and their associated chloride analogs suggests miscibility in the reacting medium.

Since the First level thermodynamic calculations indicate miscibility of all reactants, the thermodynamic calculations of reacting species in accordance with Scheme 2 were performed to show that these reacted oligomers are not expected to phase separate during the curing reaction and no visible evidence of phases in the DGEBD and DGEBA mediums are expected based on the estimated RI values. These results are given in Table SI 2.

Because the original reactants are miscible and there is no evidence of phase separation during the curing reaction, another area to consider is the distribution of oligomeric species in the DGEBD and DGEBA mediums. To focus this discussion a subset of the solubility parameter calculations for the DGEBD, DGEBA and their major oligomers are given in Table 4. Due to the larger size of the DGEBA ($m = 2$) oligomer the δ_{HD} (hydrogen donor) and δ_{HA} (hydrogen acceptor) values had to be calculated manually (Figure SI 7). The complete set of data that includes the other oligomers is given in the Supplemental Information (Table SI 1 and Table SI 2).

From the abbreviated information in Table 4, it is important to notice that the DGEBD oligomers have an increased amount of HD character relative to the DGEBD ($m = 0$) monomer. This increase is caused by the presence of the hydroxyl groups in the oligomers. Thus, these alcohol containing oligomers are protic and can be considered as being dissolved in an aprotic solvent, since the DGEBD ($m = 0$) monomer has no hydrogen bonding capability.

The DGEBD oligomers with multiple hydroxyl groups have a larger δ_{HD} that may increase the propensity of these molecules to undergo intermolecular self-association to form long-lived clusters. To investigate the clustering hypothesis a mechanophore labeled 95 mass % purity DGEBD was cured with m-PDA and the false color image is shown in Fig. 6. This image covers a larger area to ensure that no heterogeneities are missed. Comparing this figure with Fig. 5, one can readily see that the brownish/orange (shorter lifetime) regions (i.e., $\langle \tau_1 \rangle = 1.39$ ns) are absent in Fig. 6. Thus, on the macroscopic scale the network is homogeneous, and the absence of the shorter lifetime regions observed in Fig. 5 links those macroscopic heterogeneities to the oligomers found in the 60 mass % purity DGEBD.

For completeness, single pixel analyses were performed on two random pixels of the solid green image with the selected pixels shown in Figure SI 10 and the results tabulated in Table 3. Both regions were easily fit with a SEF, with the single pixel τ (τ^{SP}) values being 2.9 ns and 3.0 ns. As shown in Fig. 6, the mean value of the τ^{SP} histogram ($\langle \tau^{SP} \rangle$) is 2.8 ns with a range of values from $\tau^{SP} \approx 2.6$ ns to $\tau^{SP} \approx 3.1$ ns. Thus, the τ^{SP} values given in Table 3 fall within the range delineated by the histogram plot in Fig. 6 and leads to the conclusion that the DGEBD (95 mass % purity)/m-PDA network is also homogeneous on the molecular level.

The image also confirms our earlier assertion that the heterogeneities observed in Fig. 5 are not caused by the two fluorescent centers from the RS-mechanophore shown in Scheme 3 and discussed in the Supplemental Information (Hyperspectral Response of the Mechanophore Section). Thus, the heterogeneity in the DGEBD (60 mass % purity)/m-PDA network is associated with the oligomers that intermix during the curing process to yield a heterogeneous environ-

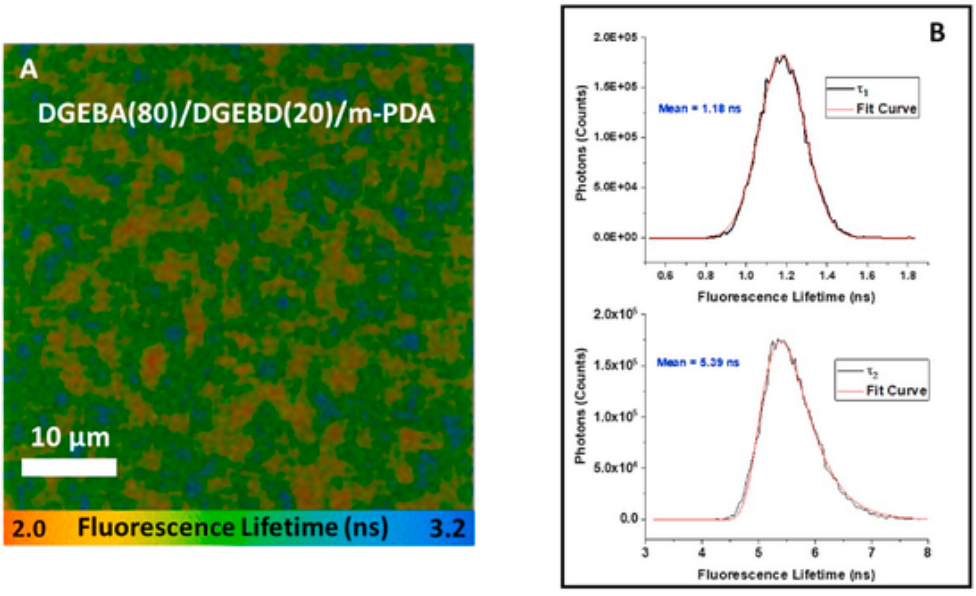

Fig. 8. (A) False color image for the photoactivated mechanophore contained in epoxy resin DGEBA (80 mass %)/DGEBD (20 mass %)/m-PDA to allow visualizing the dynamic heterogeneity of the matrix. The photon counts from each pixel (τ_m^{SP}) is based on the weighted average fluorescence lifetimes components (τ_1^{SP} and τ_2^{SP}) from the DEF. (B) Histograms for the fluorescence lifetime components [τ_1^{SP}, with mean value $\langle \tau_1 \rangle = 1.18$ ns, and τ_2^{SP}, with mean value $\langle \tau_2 \rangle = 5.39$ ns). Lower lifetimes are indicative of regions with faster local dynamics. (For interpretation of the references to color in this figure legend, the reader is referred to the Web version of this article.)

Table 3
Selected single pixel analyses from DGEBD/m-PDA networks.

False Color Region in Fig. 5 System 2 M(a)	Figure SI 9 Analysis Code	τ_m^{SP} ns	τ_1^{SP} ns	Photon Fraction	τ_2^{SP} ns	Photon Fraction
Green	B	3.3	1.2	0.638	7.0	0.362
Brownish/Orange	C	2.0	0.9	0.677	6.6	0.323

False Color Region in Fig. 6 System 2 M(b)	Figure SI 10 Analysis Code	τ_m^{SP} ns	τ^{SP} ns	Photon Fraction
Light Green	B	2.9	2.9	1.0
Dark Green	C	3.0	3.0	1.0

Table 4
Selected Solubility Parameters for DGEBD, DGEBA and major impurities.

Epoxide	Selected Solubility Parameters via HSPiP, $\sqrt{\text{MPa}}$	
	δ_{HD}	δ_{HA}
Diglycidyl ether of butandiol (DGEBD, $m = 0$), $\ell^e = 13.5$ Å	0.1	6.7
DGEBD ($m = 1, n = 0$), $\ell^e = 25.9$ Å	3.3	7.6
DGEBD ($m = 2, n = 0$), $\ell^e = 38.6$ Å	4.3	7.2
DGEBD ($m = 3, n = 0$), $\ell^e = 51.3$ Å	4.3	6.6
Diglycidyl ether of bisphenol-A (DGEBA), $\ell^e = 14.3$ Å	0.1	5.2
DGEBA ($m = 1$), $\ell^e = 22.2$ Å	1.9	3.4
DGEBA ($m = 2$), $\ell^e = 39.6$ Å	2.8	4.9
Dihydroxy DGEBA	7.6	9.4

ment at the molecular level due to the reduction in crosslink density by the self-association of the oligomers to produce the macroscopic heterogeneity observed in Fig. 5.

Self-Association and the Role of Steric Hindrance. The self-association of oligomers that may be in epoxy resins has not been extensively investigated. However, a 1985 review of E-A reaction kinetics, mechanisms, and thermodynamics by Rozenberg [16] suggested that the autocatalytic nature of the E-A reaction (Scheme 1) may be more complicated than envisioned by Smith [13]. In particular, Rozenberg indicated that the K_i reaction rates depicted in Scheme 2 could be perturbed by the presence of donor-acceptor interactions of the starting reagents with the reaction products. Noting that hydroxyl groups comprise the dominant self-association in E-A reactions, he states that cyclic associates that exist in the form of trimers (Fig. 7A) are inactive in catalysis of the nucleophilic E-A reaction depicted in Scheme 1. Of the numerous publications that have cited this review, only the 2017 dynamic light scattering research of Zhavoronok et al. [41] alludes to the existence of supramolecular structures composed of aggregates of epoxy oligomers in commercial epoxies and their blends. Since a complete characterization of the aliphatic multi-functional epoxides was not performed, definitive conclusions were not possible. However, it should be noted that the aromatic bis-epoxide DGEBA and aliphatic bis-epoxide DGEBD that are used in the current investigation has been characterized by Mijovic et al. [20] and shown to yield protic oligomers (Figure SI 1 and Figure SI 2, respectively) consistent with what is generally known about the synthesis of glycidyl ethers from aliphatic polyols [40].

Noting that the oligomers in 60 mass % DGEBD (Figure SI 2) and DGEBA (Epon 828, Figure SI 1) can be viewed as protic (alcoholic) molecules dissolved in an aprotic solvent (i.e., the DGEBD or DGEBA monomer), research related to the self-association of alcohols in aprotic solvents may be relevant. A 1996 study by Forland et al. [43] investigated the self-association of medium-chain alcohols (protic molecules) in n-dodecane (aprotic solvent) up to a OH molal concentration of 0.2 mol/kg. While acknowledging the possible existence of minor amounts of open-chain aggregates (Fig. 7C), their results indicates that monomeric alcohols are dominant in the low-molality region, while cyclic tetramers (Fig. 7D) dominate in the upper concentration range. They also observed a decrease in self-association of the cyclic tetramer and a corresponding increase in hydroxyl monomer with increasing steric hinderance around the OH group. It should be pointed out that the concentration dependence of associated alcohols in aprotic media has been known since the late 1950s [44,45].

Additionally, Bellamy and Pace [42] indicate that the cyclic dimers (Fig. 7B) have bent hydrogen bonds which are abnormally weak compared to open-chain aggregates (Fig. 7C) or cyclic trimers and tetramers (Fig. 7A and D). Hence, the cyclic trimers alluded to by Rozenberg and the cyclic tetramers suggested by Forland et al. and others [45,46] are comparable species, with both being inactive with respect to catalyzing the E-A reaction.

Since the DGEBA and DGEBD monomers are aprotic (Table 4), the dynamics of the hydroxyl containing oligomers should mimic those of the Forland et al. research. For the 60 mass % purity DGEBD and DGEBA (Epon 828) the OH molal concentrations are ≈ 1.5 mol/kg and ≈ 1.1 mol/kg, respectively. These values are well above the 0.2 mol/kg concentration investigated by Forland et al., thus, one might expect the DGEBD and DGEBA oligomers to self-associate in their respective aprotic mediums to form predominantly cyclic tetramers that are non-catalytic on the E-A reaction. This appears to be the case for 60 mass % purity DGEBD, since its reaction kinetics are slower than the 95 mass % purity DGEBD, which has an OH molal concentration of <0.2 mol/kg.

Noting that hydroxyl groups on the DGEBA oligomers are attached on two of the three carbon bonds with bulky and rigid bisphenol-A units (Figure SI 1) and recalling that the cyclic tetramer concentration is sensitive to steric hinderance, it is likely that the predominant hydroxyl species in DGEBA (Epon 828) is monomeric and available for catalysis. This assertion agrees with the scheme shown by I.T. Smith [13], and enhanced kinetics has been observed by Kotula et al. [47] for Epon 828 compared to monomeric DGEBA. This contrasts with the less hindered hydroxyl groups in oligomeric DGEBD, which are not observed to catalyze the reaction.

DGEBA (80 mass %)/DGEBD (20 mass %)/m-PDA epoxy [System 3 M]. Unlike Fig. 2A, which is the DGEBA/m-PDA image [System 1 M], the false color image in Fig. 8A, which ranges from 2.0 ns to 3.2 ns, contains only a few dark blue regions (≈ 3.2 ns). Fig. 8A consists mainly of regions that are blue/green (≈ 2.5 ns) and brownish/orange (≈ 2.0 ns). The range of lifetimes in this false color image is comparable to the DGEBD (60 mass %)/m-PDA matrix even though the T_g difference between the two networks is ≈ 70 °C. Consistent with the previous DGEBD (60 mass % purity)/m-PDA and DGEBA/m-PDA networks, the FLIM signal from each pixel (τ_m^{SP}) of the DGEBA (80 mass %)/DGEBD (20 mass %)/m-PDA network was deconvoluted into τ_1^{SP} and τ_2^{SP} values with histogram plots shown in Fig. 8B. From the plots, $\langle\tau_1\rangle = 1.18$ ns (range: $\tau_1^{SP} \approx 0.8$ ns to $\tau_1^{SP} \approx 1.6$ ns) and $\langle\tau_2\rangle = 5.39$ ns (range: $\tau_2^{SP} \approx 4.0$ ns to $\tau_2^{SP} \approx 8.0$ ns). Thus, the sub-pixel responses from the RS-mechanophores indicate a mixture of local environments that contain fast (represented by τ_1^{SP}) and slow (represented by τ_2^{SP}) molecular dynamics.

Therefore, the blended network is heterogeneous on the molecular level and consistent with the expected heterogeneity inferred from Scheme 2 when the E-A reaction involves the concurrent reaction of two bis-epoxides with an amine. To underscore this point, single pixel analysis of the three regions that encompass the macroscopic heterogeneity observed in Fig. 8 can be found in the Supplemental Information Figure SI 11 and summarized in Table 5.

As one would expect with the integration of the DGEBD molecule into the DGEBA/m-PDA network, the τ_m^{SP} values for this network are generally lower than the DGEBA/m-PDA network (compare Tables 2

Table 5
Selected Single Pixel Analyses from DGEBA (80 mass %)/DGEBD (20 mass %)/m-PDA Network.

False Color Region in Fig. 8 System 3 M	Figure SI 11 Analysis Code	τ_m^{SP}	τ_1^{SP}		τ_2^{SP}	
			ns	Photon Fraction	ns	Photon Fraction
Dark Blue	D	2.8	1.5	0.735	6.4	0.265
Blue/Green	C	2.4	1.2	0.700	5.2	0.300
Brownish/Orange	B	2.2	0.89	0.665	4.8	0.335

and 5). Thus, the molecular dynamics of this network is faster on a local level than the DGEBA/m-PDA network, even though their T_gs are similar. What is even more interesting is that the local molecular dynamics of this network is also faster than the DGEBD/m-PDA networks (compare Tables 3 and 5), despite their much lower T_gs (see Table 1).

The τ_m^{SP} histogram plot for the DGEBA (80 mass %)/DGEBD (20 mass %)/m-PDA [3 M] network (Fig. 4) has a $\langle \tau_m^{SP} \rangle \approx 2.7$ ns that arises from τ_m^{SP} values that range from ≈ 2.3 ns to ≈ 3.8 ns. Although the histogram plots for the DGEBA/m-PDA and DGEBD (60 mass %)/m-PDA are Gaussian in appearance, the τ_m^{SP} values for the DGEBA (80 mass %)/DGEBD (20 mass %)/m-PDA are skewed to higher values ≈ 3.8 ns that overlap the τ_m^{SP} range of the DGEBD/m-PDA networks and the lower range of the DGEBA/m-PDA network. It is also clear that the $\langle \tau_m^{SP} \rangle$ and the τ_m^{SP} minimum range values are much lower that either of the two previously discussed networks. This is surprising given that the T_g of this network is only 8 °C lower than the DGEBA/m-PDA network (Table 1).

Local molecular motions are a unique type of molecular mobility that exists in glassy amorphous polymers below T_g [48]. The β relaxation peak in E-A networks has been associated with the local movement (aka, crank shaft motion) of the hydroxyether fragment (i.e., –CH_2-CH(OH)–CH_2–O-) that is formed during the curing reaction. This crank shaft motion is known to be impeded energetically by hydrogen bonds that the hydroxyl groups of the hydroxyether fragment forms in the network. Existing research [49] has shown that practically all OH groups in typical E-A networks are involved in hydrogen bonding. Although the DGEBA and DGEBD monomers have similar ℓ^e values (Table SI 1), it is probable that the introduction of the more flexible DGEBD molecule into the DGEBA/m-PDA network may alter the packing density of the network and disrupt the propensity of the hydroxyether fragments to form hydrogen bonds at the molecular level. A recent perspective [50] on the effect of hydrogen bonds in E-A networks suggests that the effect of reactive diluents, such as DGEBD, on hydrogen bond disruption and packing density has not been extensively investigated.

At the macroscopic level, the brownish/orange regions have a similar τ_m^{SP} value to those observed in the DGEBD (60 mass %)/m-PDA network (compare Tables 3 and 5). Based on the inferences that can be obtained from the Forland et al. research and the DGEBD/m-PDA networks discussed previously, these regions are likely composed of the self-associating oligomers that exist in the 60 mass % purity DGEBD that is integrated into the DGEBA/DGEBD network. This self-association likely explains the decrease in the reaction rate of the DGEBA (Epon 828, 80 mass %)/DGEBD (RD-2, 20 mass %)/m-PDA curing reaction observed in the Rheo-Raman studies [47]. The previous section discussed the possibility that steric hindrance of the rigid biphenyl groups in Epon 828 DGEBA prevents the formation of cyclic hydrogen-bonded tetramers, despite the high molal concentration of OH groups (≈ 1.1 mol/kg). However, the less hindered DGEBD oligomers more readily form stable cyclic tetramers that can slow its reaction kinetics. It follows from these inferences that the DGEBA (80 mass %)/DGEBD (20 mass %)/m-PDA slow reaction kinetics may be due to the formation of mixed-cyclic tetramers composed of DGEBA and DGEBD oligomers that effectively eliminate the catalytic activity of the DGEBA oligomers in Scheme 1. Thus, most of the macroscopic heterogeneity observed in Fig. 8 appears to be due to the self-association of DGEBD and DGEBA oligomers as mixed-cyclic tetramers.

The flexibility of these oligomers and their much higher ℓ^e values will almost certainly disrupt the hydrogen bonding and packing density of the network in these regions and may be an additional source of the increased localized flexibility reflected by the τ_m^{SP} values of the DGEBA (Epon 828, 80 mass %)/DGEBD (RD-2, 20 mass %)/m-PDA network. Consistent with this interpretation, the apparent activation energy for the β relaxation ($E_{a,\beta}^{\neq}$) for this system was obtained from dynamical mechanical measurements and shown to be [15.0 ± 0.5 kcal/mol ($R^2 = 0.98$)]. This value is less than the DGEBA/m-PDA [$E_{a,\beta}^{\neq} = 17.7 \pm 0.6$ kcal/mol ($R^2 = 0.97$)] [23].

The data in Table 5 also suggests that slowing of the molecular dynamics at the pixel level, which is reflected by increasing τ_m^{SP} values, is not simply correlated at the molecular level to increasing values of τ_2^{SP} (i.e., the slow molecular dynamics parameter) and a corresponding increase in its photon fraction. As in Table 2, the increases in the photon fraction of τ_1^{SP}, which represents faster molecular dynamics, trends with increases in τ_m^{SP}, thereby leading to the previously observed counterintuitive behavior observed in the DGEBA/m-PDA network.

5. Conclusions

Strategically integrating the RS-mechanophore into the DGEBA(80 mass %)/DGEBD(20 mass %) epoxy blend [System 3 M] and the corresponding unblended networks [System 1 M and 2 M(a)], revealed through the UV activated mechanophore that all three transparent networks were heterogeneous. For System 1 M, which is the DGEBA/m-PDA network, the heterogeneity in the FLIM image (Fig. 2) is readily linked to the resin being under-cured. For the three dominant false color (pixel) regions observed in the FLIM image, the decay curves for each pixel region were fit using a DEF (Equation 1). The τ_1^{SP} and τ_2^{SP} lifetimes obtained from each fit were shown to vary with color, thereby, indicating different degrees of rigidity and flexibility within each macroscopic region and at the molecular level. Although beyond the scope of the current research, the cited research of Aoki et al. [10] suggests that the heterogeneity in the DGEBA/m-PDA network may also be observed when System 1 M is fully cured. This would further link the observed heterogeneity to inhomogeneous network formation arising from the crosslinking process as speculated by Dusek [3].

The FLIM image (Fig. 5) for the DGEBD (60 mass % purity)/m-PDA network [System 2 M] was also shown to be heterogeneous. By comparing this FLIM image with that of the DGEBD (95 mass % purity)/m-PDA network (Fig. 6), the heterogeneity in Fig. 5 was linked to the presence of the oligomers in the 60 mass % purity DGEBD, which the authors believe form long-lived clusters through self-association via the multiple hydroxyl groups on each oligomer chain, This self-association is thought to minimize the thermodynamic mismatch in the predominate $m = 0$ DGEBD medium. In addition, analysis of the pixel decay curves revealed that the DGEBD (60 mass % purity)/m-PDA network is best fit by a DEF, while the DGEBD (95 mass % purity)/m-PDA network is best fit by a SEF. This analysis also links the increased flexibility reflected in τ_1^{SP} to the oligomers.

Based on these results and literature data indicating that DGEBA reacts with amines faster than DGEBD, the heterogeneity observed in the DGEBA(80 mass %)/DGEBD(20 mass %) epoxy blend cured with m-PDA [System 3 M] is likely caused at the molecular level by reaction kinetics differences of the two bis-epoxides with m-PDA and at the macroscopic level by the self-association of the DGEBD oligomers in the 60 mass % purity DGEBD (Fig. 8). From the previous analyses, it is not surprising that the decay curves of each pixel region must be fit by a DEF. Interestingly, for System 3 M, the preponderance of regions exhibiting τ_1^{SP} lifetimes, which are associated with DGEBD, seems to exceed the

DGEBA/DGEBD molar ratio (≈2.7:1). This apparent higher concentration of τ_1 lifetimes may result in a reduction of the average FLIM lifetime of this system (≈2.7 ns) relative to the unblended DGEBA/m-PDA (≈3.6 ns) and DGEBD/m-PDA (≈3.1 ns) networks. It is probable that this decrease in lifetime may be caused by a reduced packing density and disruption in the degree of hydrogen bonding in the cured network.

The counterintuitive results observed in the heterogeneous systems suggests to the authors that rigidity in these networks may be linked to regional differences in the network's thermal expansion coefficient (CTE). Molecular dynamic simulation results on epoxy-amine systems indicate that the CTE of the network decreases with increasing crosslink density, both above and below T_g [51,52]. If the ≈ 0.33 photon fraction of τ_2^{SP} for the pixels with the highest τ_m^{SP} (e.g., in Tables 2 and 5) can be associated with the amount of rigid material within the pixel and if this rigid region is essentially surrounded by the higher photon fraction τ_1^{SP} material (≈ 0.66 photon fraction), then the mobility of the tightly crosslinked network may be further restricted as the network cools to room temperature by the surrounding loosely crosslinked or flexible networks that may have a higher CTE. A research program is currently being devised to investigate this hypothesis.

The integration of the RS-mechanophore into these transparent networks offers a wealth of new information about the morphology that results from the curing process and the role that impurities and reaction kinetics may play in morphology development. This approach provides a new tool for understanding the network of thermoset systems and potentially provides additional information that can be linked to the mechanical properties of the network.

CRediT authorship contribution statement

Jeremiah W. Woodcock : Conceptualization, Investigation, Software, Data curation, Resources, Formal analysis, Writing – original draft, Writing – review & editing, Visualization. **Stephan J. Stranick :** Conceptualization, Software. **Anthony P. Kotula :** Conceptualization, Resources, Formal analysis, Writing – review & editing, Visualization. **Shawn H. Chen :** Investigation. **Jeffrey W. Gilman :** Conceptualization. **Gale A. Holmes :** Conceptualization, Software, Resources, Data curation, Formal analysis, Writing – original draft, Writing – review & editing, Visualization, Supervision.

Declaration of competing interest

The authors declare that they have no known competing financial interests or personal relationships that could have appeared to influence the work reported in this paper.

Data availability

Data will be made available on request.

Appendix A. Supplementary data

Supplementary data to this article can be found online at https://doi.org/10.1016/j.polymer.2023.125826.

References

[1] V.B. Gupta, L.T. Drzal, W.W. Adams, R. Omlor, An electron microscopic study of the morphology of cured epoxy resin, J. Mater. Sci. 20 (10) (1985) 3439–3452.
[2] K. Dusek, J. Plestil, F. Lednicky, S. Lunak, Are cured epoxy resins inhomogeneous? Polymer 19 (4) (1978) 393–397.
[3] K. Dusek, Are cured thermoset resins inhomogeneous? Angew. Makromol. Chem. 240 (1996) 1–15.
[4] K. Dusek, Network Formation in curing of epoxy-resins, Adv. Polym. Sci. 78 (1986) 1–59.
[5] W.L. Wu, J.T. Hu, D.L. Hunston, Structural heterogeneity in epoxies, Polym. Eng. Sci. 30 (14) (1990) 835–840.
[6] A.R. Kannurpatti, J.W. Anseth, C.N. Bowman, A study of the evolution of mechanical properties and structural heterogeneity of polymer networks formed by photopolymerizations of multifunctional (meth)acrylates, Polymer 39 (12) (1998) 2507–2513.
[7] A.S. Sridhar, Effect of stoichiometry on crosslinked epoxy resin characteristics: structural heterogeneities, topological defects, properties, free volume and segmental mobility, Soft Matter 18 (12) (2022) 2354–2372.
[8] S. Morsch, Y.W. Liu, S.B. Lyon, S.R. Gibbon, Insights into epoxy network nanostructural heterogeneity using AFM-IR, ACS Appl. Mater. Interfaces 8 (1) (2016) 959–966.
[9] H. Kishi, T. Naitou, S. Matsuda, A. Murakami, Y. Muraji, Y. Nakagawa, Mechanical properties and inhomogeneous nanostructures of dicyandiamide-cured epoxy resins, J. Polym. Sci. B Polym. Phys. 45 (12) (2007) 1425–1434.
[10] M. Aoki, A. Shundo, R. Kuwahara, S. Yamamoto, K. Tanaka, Mesoscopic heterogeneity in the curing process of an epoxy-amine system, Macromolecules 52 (5) (2019) 2075–2082.
[11] E. Urbaczewski, J.-P. Pascault, H. Sautereau, C.C. Riccardi, S.S. Moschiar, R.J.J. Williams, Influence of the addition of an aliphatic epoxide as reactive diluent on the cure kiinetics of epoxy/amine formulations, Makromol. Chem. 191 (4) (1990) 943–953.
[12] E. Urbaczewski-Espuche, J. Galy, J.-F. Gerard, J.-P. Pascault, H. Sautereau, Influence of chain flexibility and crosslink density on mechanical properties of epoxy/amine networks, Polym. Eng. Sci. 31 (22) (1991) 1572–1580.
[13] I.T. Smith, The mechanism of the crosslinking of epoxide resins by amines, Polymer 2 (1) (1961) 95–108.
[14] K. Dusek, M. Ilavsky, S. Lunak, Curing of epoxy-resins .1. Statistics of curing of diepoxides with diamines, J. Polym. Sci. Part C-Polymer Symposium (53) (1975) 29–44.
[15] L. Shechter, J. Wynstra, R.P. Kurkjy, Glycidyl ether reactions with amines, Ind. Eng. Chem. 48 (1) (1956) 94–97.
[16] B.A. Rozenberg, in: K. Dusek (Ed.), Epoxy Resins and Composites II: Kinetics, Thermodynamics and Mechanism of Reactions of Epoxy Oligomers with Amines, Springer-Verlag, Berlin, 1985, pp. 113–165.
[17] A. Periasamy, R.N. Day, Molecular Imaging: FRET Microscopy and Spectroscopy, Oxford University Press, Oxford, 2005.
[18] A.M. Shibley, Filament winding, in: G. Lubin (Ed.), Handbook of Composites, Van Nostrand Reinhold Company Inc., New York, 1982, pp. 449–478.
[19] G.L. Hagnauer, in: A.M.a.M.R. Center (Ed.), HPLC and GPC Analysis of Epon Epoxy Resins, U.S. Army MaterielDevelopment and Readiness Command, 1979, pp. 1–22 Watertown, MA.
[20] E.M. Pearce, J. Mijovic, Characterization-Curing-Property Studies of HBRF 55A Resin Formulations, 1985, pp. 1–134 New York.
[21] J.W. Woodcock, R.J. Sheridan, R. Beams, S.J. Stranick, W.F. Mitchell, L.C. Brinson, V. Gudapati, D. Hartman, A. Vaidya, J.W. Gilman, G.A. Holmes, Damage Sensing Using a Mechanophore Crosslinked Epoxy Resin in Single-Fiber Composites, Composites Science and Technology, 2020.
[22] G.A. Holmes, The potential impact of DGEBA/amine reaction kinetics on interphase formation in glass fiber composites, Compos. Sci. Technol. 168 (2018) 437–447.
[23] M.C. Richardson, J.H. Kim, J.W. Woodcock, J.W. Gilman, G.A. Holmes, The search for structural heterogeneity in amine-cured epoxy/epoxy thermosets. Dynamic mechanical analysis, J. Mater. Sci. WERB Rev. (2022) PUBID G2021-1373).
[24] P.J. Herrera-Franco, L.T. Drzal, Comparison of methods for the measurement of fibre/matirx adhesion in composites, Composites 23 (1) (1992) 2–27.
[25] T.T. Chiao, E.S. Jessop, H.A. Newey, An epoxy system for filament winding, SAMPE Q. 6 (1) (1974) 28–32.
[26] K.C.B. Lee, J. Siegel, S.E.D. Webb, S. Leveque-Fort, M.J. Cole, R. Jones, K. Dowling, M.J. Lever, P.M.W. French, Application of the stretched exponential function to fluorescence lifetime imaging, Biophys. J. 81 (3) (2001) 1265–1274.
[27] D. Woll, E. Braeken, A. Deres, F.C. De Schryver, H. Uji-i, J. Hofkens, Polymers and single molecule fluorescence spectroscopy, what can we learn? Chem. Soc. Rev. 38 (2) (2009) 313–328.
[28] E.B. van Munster, T.W.J. Gadella, Fluorescence lifetime imaging microscopy (FLIM), in: J. Rietdorf (Ed.), Microscopy Techniques2005, pp. 143-175.
[29] R. Datta, T.M. Heaster, J.T. Sharick, A.A. Gillette, M.C. Skala, Fluorescence lifetime imaging microscopy: fundamentals and advances in instrumentation, analysis, and applications, J. Biomed. Opt. 25 (7) (2020).
[30] H.S. Chu, J.C. Seferis, Network structure description and analysis of amine-cured epoxy matrices, in: J.C. Seferis, L. Nicolais (Eds.), The Role of the Polymeric Matrix in the Processing and Structural Properties of Composite Materials, Plenum Press, New York, 1983, pp. 53–125.
[31] Y. Li, S. Natakorn, Y. Chen, M. Safar, M. Cunningham, J. Tian, D.D.-U. Li, Investigations on average fluorescence lifetimes for visualizing multi-exponential decays, Front. Phys. 8 (2020).
[32] D.R. James, W.R. Ware, A fallacy in the interpretation of fluorescence decay parameters, Chem. Phys. Lett. 120 (4–5) (1985) 455–459.
[33] W. Becker, The Bh TCSPC Handbook, ninth ed., Becker & Hickl GmbH, Berlin, 2021.
[34] A. Sillen, Y. Engelborghs, The correct use of “average” fluorescence parameters, Photochem. Photobiol. 67 (1998).
[35] L.A. Kleintjens, R. Koningsveld, Thermodynamics of polymer solutions and blends, Die Makromolekulare Chemie Macromolecular (1) (1988) 203–214 Symposia 20/21.
[36] S. Abbott, C.M. Hansen, H. Yamamoto, R.S. Valpey III, Hansen Solubility Parameters in Practice, fifth ed., Hansen-Solubility.com, 2015.
[37] D. Rappoport, N.R.M. Crawford, F. Furche, K. Burke, Approximate density

functionals: which should I choose from? in: E.I. Solomon, R.B. King, R.A. Scott (Eds.), Computational Inorganic and Bioinorganic Chemistry, John Wiley & Sons Ltd, Chichester, 2009, pp. 159–172.
[38] D.A. McQuarrie, J.D. Simon, Physical Chemistry: A Molecular Approach, University Science Books, Sausalito, CA, 1997.
[39] D.W. Schiering, J.E. Katon, L.T. Drzal, V.B. Gupta, An infrared spectroscopic investigation of the curing reactions of the epon-828 meta-phenylenediamine system, J. Appl. Polym. Sci. 34 (7) (1987) 2367–2375.
[40] H. Lee, K. Neville, Handbook of Epoxy Resins, McGraw-Hill Book Company, New York, 1967.
[41] E.S. Zhavoronok, I.N. Senchikhin, V.V. Vysotskii, V.I. Roldugin, Effect of the nature and associate structure of an epoxy oligomer on the rate of its curing with diamine, Polym. Sci. B 59 (4) (2017) 421–429.
[42] L.J. Bellamy, R.J. Pace, Hydrogen bonding by alcohols and phenols .I. The nature of the hydrogen bond in alcohol dimers and polymers, Spectrochim. Acta 22 (3) (1966) 525.
[43] G.M. Forland, F.O. Libnau, O.M. Kvalheim, H. Hoiland, Self-association of medium-chain alcohols in n-decane solutions, Appl. Spectrosc. 50 (10) (1996) 1264–1272.
[44] L.P. Kuhn, R.E. Bowman, The hydrogen bond .4. Intramolecular hydrogen bonding in triols, Spectrochim. Acta 17 (6) (1961) 650–660.
[45] W.C. Coburn, E. Grunwald, Infrared measurements of the association of ethanol in carbon tetrachloride, J. Am. Chem. Soc. 80 (6) (1958) 1318–1322.
[46] M. Saunders, J.B. Hyne, Trimeric association of tert-butanol by NMR, J. Chem. Phys. 29 (1) (1958) 253–254.
[47] A.P. Kotula, J.W. Woodcock, J.W. Gilman, G.A. Holmes, A Cure Kinetics Investigation of Amine-Cured Epoxy by Rheo-Raman Spectroscopy, Polymer Submitted for Review, 2023.
[48] S.N. Rudnev, E.F. Oleinik, Low-temperature molecular motions in crosslinked epoxide polymeric systems, Polym. Sci. 22 (11) (1980) 2723–2734.
[49] R. Dave, M.P. Dudukovic, H. Furukawa, T. Kamon, J.L. Kardos, E.S.-W. Kong, E.F. Oleinik, S.D. Senturia, N.F. Sheppard Jr, in: K. Dusek (Ed.), Epoxy Resins and Composites IV, Springer-Verlag, Berlin, 1987, pp. 1–218.
[50] A.-S. Mora, R. Tayouo, B. Boutevin, G. David, S. Caillol, A perspective approach on the amine reactivity and the hydrogen bonds effect on epoxy-amine systems, Eur. Polym. J. 123 (2020) 109460.
[51] A. Bandyopadhyay, P.K. Valavala, T.C. Clancy, K.E. Wise, G.M. Odegard, Molecular modeling of crosslinked epoxy polymers: the effect of crosslink density on thermomechanical properties, Polymer 52 (11) (2011) 2445–2452.
[52] S. Masoumi, B. Arab, H. Valipour, A study of thermo-mechanical properties of the cross-linked epoxy: an atomistic simulation, Polymer 70 (2015) 351–360.